Anatomy of Demagnetizing and Exchange Fields in Magnetic Nano-Dots Influenced by 3D Shape Modifications

T Blachowicz[1,3] **and A Ehrmann**[2, 3]
[1] Institute of Physics – Center for Science and Education, Silesian University of Technology, 44-100 Gliwice, Poland
[2] Faculty of Textile and Clothing Technology, Niederrhein University of Applied Sciences, 41065 Mönchengladbach, Germany
[3] VIARAM – Virtual Institute for Applied Research on Advanced Materials
E-mail: tomasz.blachowicz@polsl.pl

Abstract. Hysteresis loops of 3D ferromagnetic permalloy nano-half-balls (dots) with 100 nm base diameter have been examined by means of LLG micromagnetic simulations and finite element methods. Tests were carried out with two orthogonal directions of the externally applied field at 10 kA/(m.ns) field sweeping speed. The comparison of samples with different 3D modifications at the sub-10nm scale, accessible by nowadays lithographic techniques, enables conclusions about different mechanisms of competition between demagnetizing and exchange fields. Design paradigms provided here can be applied, e.g., in bit-patterned media used as novel magnetic storage systems.

1. Introduction

Analysis of the microscopic structure of magnetic states plays an important role in understanding magnetic states in low dimensional objects, which is necessary for the development of nanostructures with novel features. Round objects, especially nano-dots, are of particular interest due their use in bit-patterned media [1]. Observed in nano-dots and rings, flux-closure states, vortexes, and onion states were extensively investigated in many experimental works [2-6]. First experiments with thin magnetic films on non-magnetic spheres with diameters between 20 and 1000 nm underline the importance of probing 3D nano-magnets [7-8]. The 3D nano-objects can principally be structured with today's techniques inspired by biologically self-assembled processes using proper (smart) components [9].

2. Mathematical Model

The idea of the study presented here is based on the effect that for small magnetic elements the shape modifications – due to dipolar interactions – play a crucial role in magnetization dynamics; however, due to reduced dimensionality, the demagnetizing fields can compete with exchange fields leading to specific magnetic behavior, such as oscillations, rapid transient states, and quasi-static states.

Thus, we theoretically examine 3D ferromagnetic half-balls made of commonly applied permalloy (Py) with different shape modifications in order to support development of new 3D performance paradigms. In our samples the circular base of diameter 100 nm is located in the x-y-plane. In some of the half-balls, a perpendicular hole of diameter 50 nm has been cut in order to extract the core region of a possible magnetic vortex state which is known to have a comparable diameter [10]. In that way the samples represent all basic shape features to be met in 3D-fabricated nanomagnets: planes, curved surfaces, straight and bent edges, as well as intentionally introduced cuts and holes. In order to narrow

the analysis to magnetostatic vs. exchange-based competition, magnetocrystalline anisotropy is excluded. All deviations from an ideal half-ball, created in different ways, can be seen in Fig. 1.

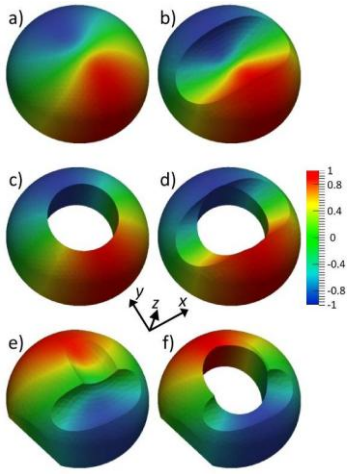

Figure 1. The samples under simulation: (a), (b) and (e) are solid half-balls, while (c) and (d) half-balls possess a 50 nm diameter hole, respectively. The height of the half-ball (a) equals 50 nm. The cylindrical cuts in the x-y plane (b, d) have 50 nm diameter, and the maximum depth of a cut, seen along the half-ball z-axis, equals 25 nm with respect to the top point of the bulk half-ball (a). Samples (e) and (f) possess arbitrary, asymmetrical cuts, and the elliptical hole in (f) case is not parallel to the z-axis. The surface x-components of magnetization, at zero-valued externally applied magnetic field, are color-coded.

Here we report results of hysteretic behavior of the half-balls using micromagnetic simulations [11], allowing for an insight into the magnetic properties, basing on the Landau-Lifshitz-Gilbert (LLG) equation of motion

$$\frac{\partial \vec{J}}{\partial t} = -\frac{\gamma}{1+\alpha^2}\vec{J}\times\vec{H}_{eff} - \frac{\gamma\alpha}{\left(1+\alpha^2\right)J_s}\vec{J}\times\left(\vec{J}\times\vec{H}_{eff}\right), \tag{1}$$

where $\vec{J}$ is the magnetic polarization vector, J_s is the magnetization polarization at saturation, γ is the electron gyromagnetic ratio, α is the damping parameter, and $\vec{H}_{eff}$ is the effective magnetic field. The effective field, in general, is a superposition of four contributing fields: the externally applied field, the magnetocrystalline field, the demagnetizing field, and the exchange field, namely

$$\vec{H}_{eff} = \vec{H}_{ext} + \frac{2K_1}{J_s}\vec{n}\left(\vec{n}\cdot\frac{\vec{J}}{J_s}\right) + \vec{H}_{demag} + \frac{2A}{J_s}\Delta\left(\frac{\vec{J}}{J_s}\right), \tag{2}$$

where K_1 is the magnetocrystalline anisotropy constant, $\vec{n}$ is the unit vector pointing in the magnetic easy-axis direction, and A is the exchange constant.

For the simulations, the MagPar [12] LLG micromagnetic solver was used, dynamically integrating the equation of motion. Finite elements were meshed as tetrahedral elements with dimensions of maximal 3.7 nm, which is smaller than the Py exchange length of 5.7 nm [11]. Near the edges, meshing was approximately 10 times denser, to include the influence of demagnetizing fields more exactly. Else, we chose the exchange constant A=1.05·10^{-11} J/m, the magnetic polarization at saturation J_s =1 T, and the Gilbert damping constant α = 0.01 [11].

3. Results and Discussion – Hysteresis Loops

Hysteresis loops have been examined with the external magnetic field H_{ext} applied along the x-axis (in the sample plane) and along the z-axis (perpendicular to the base plane), respectively. In all cases, starting from a random state of magnetization at H_{ext} = 0, the field has been changed with constant speed of 10 kA/(m.ns) up to 450 kA/m (H_{ext} along x-axis) or to 600 kA/m (H_{ext} along z-axis), respectively (this step is not shown in the graphs for clarity). Next, starting from positive saturation,

the field has been swept at a constant speed of -10 kA/(m.ns) to -450 kA/m (H_{ext} along x-axis) or to -600 kA/m (H_{ext} along z-axis), respectively. In order to close the hysteresis loops, the field has been swept back from negative to positive saturation with the same constant speed afterwards. This field sweeping speed is correlated to typical values for magneto-electronic applications [11].

3.1 Hysteresis loops for the in-plane applied field (x-direction)

The hysteresis loops obtained for H_{ext} applied along the x-axis are shown in Fig. 2. For the solid half-ball (Fig. 2a), it should be mentioned that the start of the magnetization reversal before H_{ext} = 0 is reached. Such a behavior has also been observed, e.g., by He *et al.* and interpreted as the beginning of a magnetic vortex state formation [6]. Our simulation strongly supports this interpretation, as can be seen in Fig. 2a where snapshots of the magnetization in z-direction are presented, showing vortex formations correlated with the start of the oscillations. A detailed analysis of the oscillation frequencies will be given in a future article.

While cutting the top of the solid half-ball suppresses magnetization reversal before H_{ext} = 0 (Fig. 2b), a hole in the sphere (Fig. 2c) significantly enhances the coercivity as well as the field region between first and second step of the complete magnetization reversal. This broad step is correlated with a flux-closed vortex state, while the saturation magnetization states and the oscillatory region are associated with two different onion states. The snapshots for the magnetization reversal from positive to negative saturation show the z-components of the magnetization. The oscillation here is not circular but a symmetric oscillation with the two colored domain walls oscillating towards each other and back again. Following the snapshots of the x-component of the magnetization from negative to positive saturation, the magnetization reversal from the original onion state along a second onion state to the vortex state and finally to the reversed saturated onion state is clearly visible.

However, additional top cuts in a sphere with a hole (Fig. 2d) reduce the coercivity again, which is opposite to the finding in solid half-balls. Obviously, both effects have to be taken into account if a certain coercive field is desired.

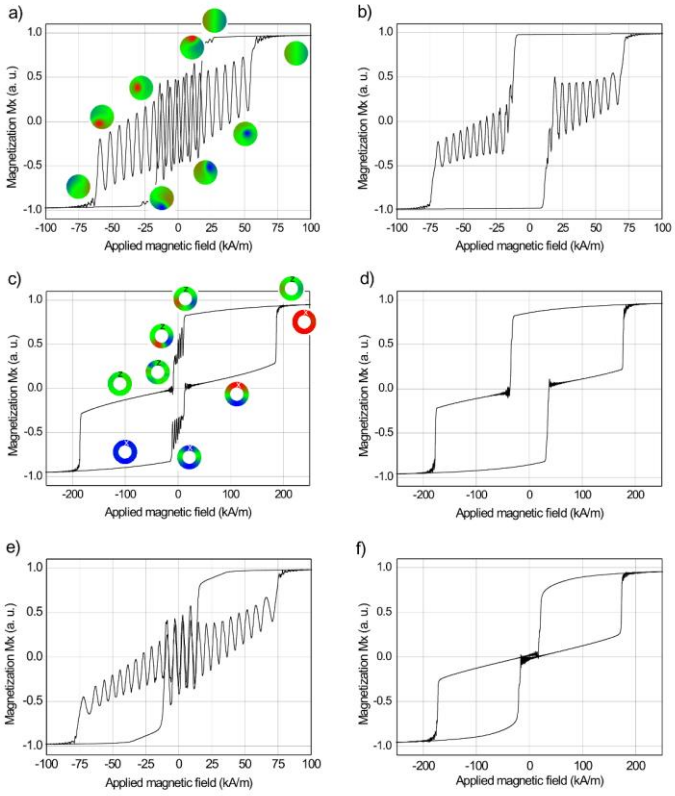

Figure 2. Hysteresis loops, simulated for the samples depicted in figure 1, for the external field applied along the x-axis. The color-coded insets in (a) show the z-component of the magnetization for different external fields, the insets in (c) exhibit the z-components (for field sweep from positive to negative values) and x-components (for field sweep from negative to positive saturation), respectively.

3.2 Hysteresis loops for the field applied perpendicular to a base-plane (z-direction)

Figure 3 shows hysteresis loops for H_{ext} applied along the z-axis. There are two types of reversal processes obtained, those with a step (Figs. 3a, 3b, and 3e) and those with smooth dynamics (Figs. 3c, 3d, and 3f). The insets in Fig. 3a show that in the solid half-ball a vortex core is built [13], which is separated from the outer part of the vortex by a circular domain wall. During the magnetization reversal process, the core region becomes smaller, while the outer ring reverses. The oscillatory step finalizes the reversal by switching the core region. Both reversal processes from positive to negative saturation and vice versa differ by the orientation of the core and the outer region.

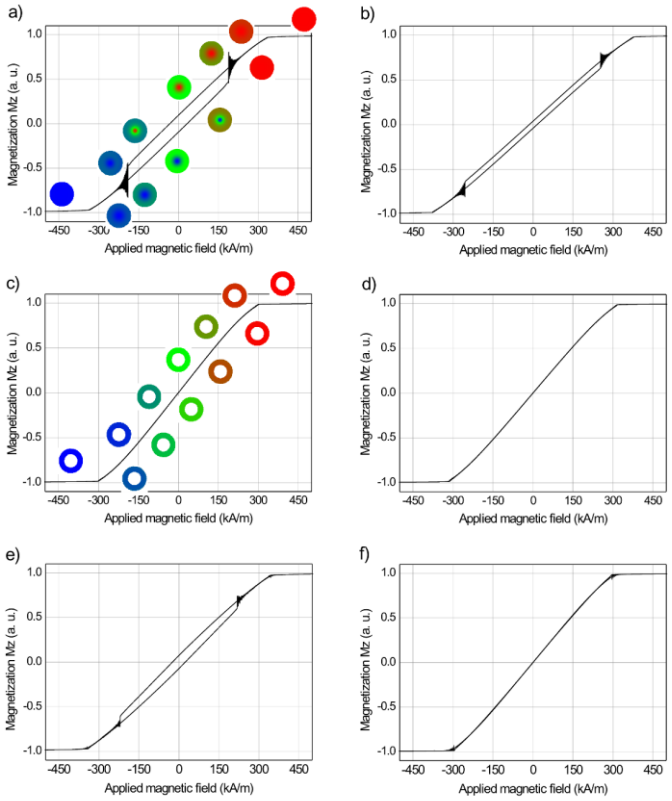

Figure 3. Hysteresis loops, simulated for the samples depicted in figure 1, for the external field applied along the z-axis. The color-coded insets in (a) and (c) show the z-component of the magnetization for different external fields.

Apparently, the cylindrical cuts in the solid half-balls (Figs. 3b and 3e) lead to smaller coercivities and remanences, while the holes (Figs. 3c, 3d, and 3e) produce smooth reversible magnetization curves. Such a reversible magnetization curve of quasi-spherical Fe particles of diameter 200 nm has also been found by Diao *et al*. [14]. However, investigation of the magnetization dynamics [13] and the color-coded insets in Fig. 3c shows that here a flux-closed state is generated, corresponding to two possible states with flux rotational direction clockwise or counter-clockwise, enabling the utilization of these nano-magnets in storage devices as well. During the magnetization reversal process, the magnetization values as well as the color-coded snapshots are identical for all external fields; the process is completely reversible.

Moreover, comparing Figs. 2 and 3, it is obvious that for the Py half-balls, the hard axis is always directed along the z-axis, as in 2D nano-magnets.

All the observed effects can be more deeply understood by considering Fig. 4, where both competing fields are visualized. It can be recognized that an additional horizontal cut increases the in-plane (x-y) components of the demagnetizing field blocking the exchange field precessions. A more detailed examination of demagnetizing and exchange energy is given in [15].

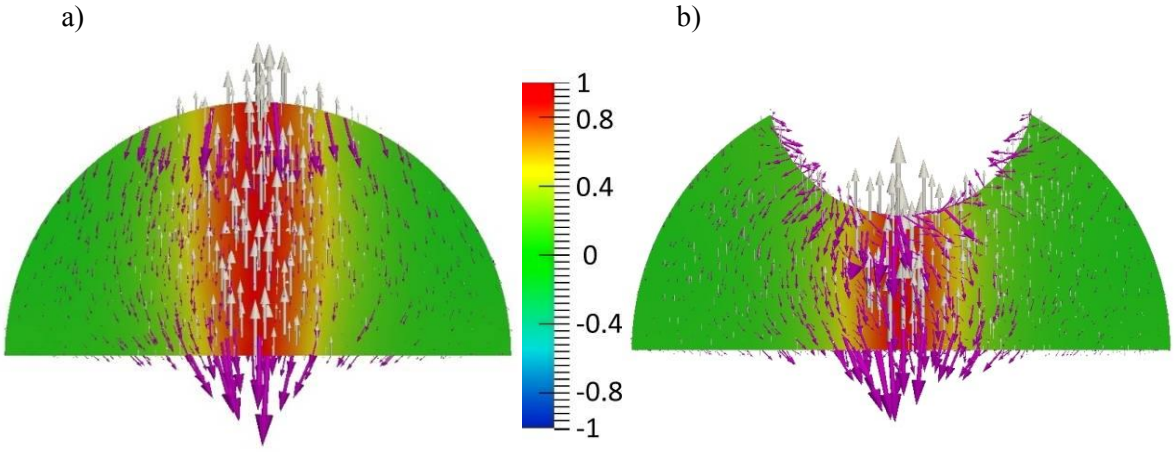

Figure 4. Visualizations of cross-sections of competing demagnetizing (dark lilac arrows) and exchange fields (light grey arrows) for the full solid sample (a) and the sample with a single horizontal cut (b). The colors at cross-sections represent local values of the M_z magnetization component: 1 (red) – vector parallel to z-axis, 0 (green) – vector perpendicular to z-axis, -1 (blue) – vector antiparallel to z-axis. The figure represents zero-valued external-field state (remanence).

4. Conclusion

In summary, we have provided some basic nanomagnetic sample 3D paradigms and given an overview about magnetization characteristics which can be reached by changes in the geometry of magnetic nano-particles, enabling deeper understanding of desired properties in a relatively broad range of modifications to meet the challenges of new 3D technology of magnetic devices. This could give an opportunity for new applications in magneto-electronics.

References

[1] Richter H, Dobin A, Heinonen O, Gao K, Veerdonk R, Lynch R, Xue J, Weller D, Asselin P, Erden M and Brockie R 2006 *IEEE Trans. Magn.* **42** 2255-60
[2] Cowburn R P, Koltsov D K, Adeyeye A O, Welland M E and Tricker D M 1999 *Phys. Rev. Lett.* **83** 1042
[3] Zhu J G, Zheng Y F and Prinz G A 2000 *J. Appl. Phys.* **87** 6668
[4] Zhu F Q, Fan D L, Zhu X C, Zhu J G, Cammarata R C and Chien C L 2004 *Adv. Mater.* **16** 2155
[5] Zhang W and Haas S 2010 *Phys. Rev. B* **81** 064433
[6] He K, Smith D J and McCartney M R 2010 *J. Appl. Phys.* **107** 09D307
[7] Soares M M, de Biasi E, Coelho L N, dos Santos M C, de Menezes F S, Knobel M, Sampaio L C and Garcia F 2008 *Phys. Rev. B* **77** 224405
[8] Amaladass E, Ludescher B, Schütz G, Tyliszczak T, Lee M S and Eimüller T 2010 *J. Appl. Phys.* **107** 053911
[9] Leong T G, Zarafshar A M and Gracias D H 2010 *Small* **6** 792
[10] Chou K W, Puzic A, Stoll H, Dolgos D, Schütz G, van Waeyenberge B, Vansteenkiste A, Tyliszczak T, Woltersdorf G and Back C H 2007 *Appl. Phys. Lett.* **90** 202505
[11] Smith N, Markham D and la Tourette D 1989 *J. Appl. Phys.* **65** 4362
[12] Scholz W, Fidler J, Schrefl T, Suess D, Dittrich R, Forster H and Tsiantos V 2003 *Comp. Mat. Sci.* **28** 366
[13] Blachowicz T, Ehrmann A, Steblinski P and Pawela L 2010 *J. Appl. Phys.* **108** 123906
[14] Diao Z, Abid M, Upadhyaya P, Venkatesan P and Coey J M D 2010 *J. Magn. Magn. Mat.* **322** 1304
[15] Ehrmann A, *Examination and simulation of new magnetic materials for the possible application in memory cells*, Logos Verlag, Berlin / Germany 2014, ISBN 978-3-8325-3772-2